Sahel Droughts Induced by Large Volcanic Eruptions Over the Last Millennium in PMIP4/Past1000 Simulations

Julian Villamayor, Myriam Khodri, Shih-Wei Fang, Johann Jungclaus, Claudia Timmreck, Davide Zanchettin

AGU ADVANCING EARTH AND SPACE SCIENCE

Geophysical Research Letters®

RESEARCH LETTER
10.1029/2022GL101478

Sahel Droughts Induced by Large Volcanic Eruptions Over the Last Millennium in PMIP4/Past1000 Simulations

J. Villamayor[1,2], M. Khodri[1], S.-W. Fang[3], J. H. Jungclaus[3], C. Timmreck[3], and D. Zanchettin[4]

[1]LOCEAN-IPSL, Sorbonne Université/CNRS/IRD/MNHN, Paris, France, [2]Now at Department of Atmospheric Chemistry and Climate, IQFR-CSIC, Madrid, Spain, [3]Max-Planck-Institut für Meteorologie, Hamburg, Germany, [4]University Ca' Foscari of Venice, Venice, Italy

Key Points:

- Climate model simulations of the past millennium show Sahel drought in response to large volcanic eruptions up to the following 2 years
- The mechanisms leading to the Sahel drying are different if it responds to extra-tropical or tropical eruptions
- The increasing frequency of eruptions throughout the past millennium modulates Sahel precipitation variability on multi-decadal timescales

Supporting Information:

Supporting Information may be found in the online version of this article.

Correspondence to:

J. Villamayor,
jvillamayor@iqfr.csic.es

Citation:

Villamayor, J., Khodri, M., Fang, S.-W., Jungclaus, J. H., Timmreck, C., & Zanchettin, D. (2023). Sahel droughts induced by large volcanic eruptions over the last millennium in PMIP4/past1000 simulations. *Geophysical Research Letters*, *50*, e2022GL101478. https://doi.org/10.1029/2022GL101478

Received 24 NOV 2022
Accepted 9 FEB 2023

Author Contributions:

Conceptualization: J. Villamayor, M. Khodri, S.-W. Fang, J. H. Jungclaus, C. Timmreck, D. Zanchettin
Formal analysis: J. Villamayor
Methodology: J. Villamayor, M. Khodri
Supervision: M. Khodri
Visualization: J. Villamayor
Writing – original draft: J. Villamayor
Writing – review & editing: M. Khodri, S.-W. Fang, J. H. Jungclaus, C. Timmreck, D. Zanchettin

Abstract This work provides evidence of the influence of large volcanic eruptions on Sahel rainfall relying on PMIP4/past1000 multi-model simulations, covering the last millennium. A classification of volcanic eruptions in the last millennium according to the meridional symmetry of the associated radiative forcing reveals different mechanisms of the West African Monsoon response at inter-annual timescale. In all cases, these simulated changes result in Sahel drying up to 2 years after an eruption. Besides, we add evidence of a role of varying volcanic activity across the past millennium in the Sahel precipitation variability at multi-decadal to secular timescales.

Plain Language Summary Relying on climate simulations of the past millennium, this work shows that the largest volcanic eruptions documented induce different mechanisms in the West African Monsoon response depending on whether the eruption occurs at extra-tropical or tropical latitudes. In both cases, such volcanic impacts can induce droughts the two following rainy seasons in the West African Sahel region. Moreover, we show first evidence of an influence of the frequency of volcanic eruptions on the Sahel precipitation regime over decades to centuries across the past millennium.

1. Introduction

The West African Sahel region is the semiarid border between the Sahara desert and the tropical savannah. Its precipitation regime is linked to the West African Monsoon (WAM), with a well-defined rainy season between July and September (JAS) (e.g., Nicholson, 2013). However, the Sahel rainfall regime has undergone dramatic changes in the 20th century, primarily linked to the sea surface temperature (SST) variability (Folland et al., 1986; Giannini et al., 2003; Park et al., 2015). At inter-annual timescale, precipitation variability is primarily associated with El Niño-Southern Oscillation (ENSO) (Rodríguez-Fonseca et al., 2015) while the Atlantic Multi-decadal Variability (AMV) can affect decadal rainfall variability and trends (Knight et al., 2006). The role of anthropogenic forcing has also been explored, such as the effect of increasing atmospheric carbon dioxide (Biasutti, 2013; Gaetani et al., 2017), the role of land use changes in amplifying precipitation variations (Kucharski et al., 2013; Zeng & Neelin, 1999) and tropospheric aerosols in driving SST and rainfall changes (Ackerley et al., 2011; Haywood et al., 2013). Yet, volcanic eruptions over the 20th century are also found to impact the Sahel rainfall (Haywood et al., 2013; Jacobson et al., 2020).

As a major natural precursor influencing global climate (McGregor et al., 2015), explosive volcanic eruptions eject large amounts of sulfur gasses into the stratosphere and form aerosol clouds, which persist there for a couple of years to increase the Earth's albedo by reflecting solar radiation (Robock, 2000). Consequently, surface and tropospheric cooling occurs in post-eruption years, amplified by water vapor feedbacks (Soden et al., 2002). The climate impact depends on the height reached by the ejections and the aerosol cloud distribution, respectively determined by the eruption's explosivity, season and latitude. Tropical eruptions induce more symmetrical forcing across the equator and global impact on surface temperature, while extra-tropical eruptions lead to inter-hemispheric asymmetric forcing and impact predominantly the own hemisphere (Timmreck, 2012).

Most work about volcanic impact on hydroclimate focuses on the hemispheric asymmetry of the forcing, which induces strong inter-hemispheric energetic imbalance and ITCZ shifts (Colose et al., 2016; Erez & Adam, 2021), although large tropical eruption clouds lead to decreased monsoon precipitation and tropical circulation changes (D'Agostino & Timmreck, 2022). The strongest eruptions over the 20th century in the Northern Hemisphere

(NH) have been associated with Sahel drought in the following couple of years, while Southern Hemisphere (SH) eruptions result in more rainfall (Haywood et al., 2013). Yet, past reconstructions of volcanic forcing show larger eruptions over the past millennium compared to the 20th century and a wider variety of erupting volcanoes (Toohey & Sigl, 2017). Hence, the observational period is not representative of volcanic forcing of the Common Era (CE) in terms of magnitude, location and eruptions frequency. In turn, reconstructed indices of the 19th century Sahel precipitation show evidence of more pronounced variability than in the 20th century (Nicholson et al., 2012), suggesting a link with concurrent large volcanic activity (Gallego et al., 2015). Reconstructions of the Nile River flow also add evidence for a significant volcanic impact on the African monsoon over the past millennium (Manning et al., 2017; Oman et al., 2006). Therefore, studying eruptions over the past millennium provides better representativeness of the variety of volcanic events and the impact on Sahel precipitation.

Understanding the consequences of historical eruptions on climate is crucial for accurately attributing the observed variability and constraining the potential climatic effects of future eruptions (Lüning et al., 2018; Man et al., 2021; Tejedor et al., 2021). This work assesses the volcanic impact on Sahel precipitation over the last millennium (850–1849 CE) relying on state-of-the-art coupled global climate model (GCM) simulations aiming at (a) finding different WAM inter-annual responses to strong volcanic eruptions depending on the latitudinal distribution of the radiative forcing, (b) characterizing the leading mechanisms and (c) discussing decadal to secular Sahel rainfall variability in association with volcanic forcing.

2. Data and Methods

This study uses the past millennium (past1000; Jungclaus et al., 2017) simulations run by the IPSL-CM6A-LR (Boucher et al., 2020; Lurton et al., 2020) and the MPI-ESM1-2-LR (Mauritsen et al., 2019; van Dijk et al., 2022) GCMs, participating in the Paleoclimate Modeling Intercomparison Project phase 4 (PMIP4; Kageyama et al., 2018) and the Coupled Model Intercomparison Project phase 6 (CMIP6; Eyring et al., 2016) (overview in Table S1 in Supporting Information S1). Ensembles of respectively three and two members are provided by these models and employed in this work. Pre-industrial control (piControl) runs are used to calculate the climatology and quantify the internal climate variability.

Presently, PMIP4 past1000 simulations using four different models are available. We focus here on the IPSL-CM6A-LR and MPI-ESM1-2-LR past1000 simulations since they consistently include a long-term volcanic forcing reconstruction of zonal and monthly mean aerosol optical depth (AOD) and effective radius compiled from the evolv2k data set (Toohey & Sigl, 2017) with the Easy Volcanic Aerosol (EVA) forcing generator (Toohey et al., 2016). Then, a selection of strong volcanic events was made based on the stratospheric AOD at 550 nm as follows: extra-tropical NH (ETNH) and tropical (TROP) eruptions are classified as strong when the mean AOD across, respectively, 45°N–90°N and 16°S–16°N peaks above the global-mean AOD and exceeds the threshold of 0.1, that is, the magnitude of a Pinatubo-like eruption (Figure 1a). No extra-tropical SH (90°S–45°S) events were found with this criterion. An estimate of the magnitude of the radiative forcing is computed as the annual global-mean anomaly of the net short-wave radiation at the top of the atmosphere (TOA). Then, the first post-eruption years are defined as those showing maximum radiative forcing anomaly following the start of selected eruptions (Table S2 in Supporting Information S1). Although the MRI-ESM2-0 and MIROC-ES2L PMIP4/past1000 model simulations use different strategies in the volcanic forcing implementation (Table S1, Figures S1 and S2 in Supporting Information S1), they were also analyzed for decadal and secular scale variability of Sahel precipitation.

After the classification of volcanic events, composites of different fields (i.e., precipitation, temperature, wind, velocity potential and specific humidity) are computed as the mean anomalies relative to the piControl climatology across the selected events. To highlight surface temperature gradients underlying the overall volcanic radiative cooling (Khodri et al., 2017), composites of relative (i.e., with respect to the 16°S–16°N mean) surface temperature anomalies are also represented. The confidence interval of the mean across all composite members is assessed with a Student *t*-test and the forcing effect on the composite anomalies relative to the internal variability is statistically evaluated by bootstrapping the unperturbed piControl anomalies.

In order to characterize the simulated variability of the Sahel mean precipitation, an inter-annual summer Sahel precipitation index (SAHELPI) is defined as the JAS mean precipitation anomalies, area-weighted and averaged across 17.5°W–10°E; 10°N–17.5°N.

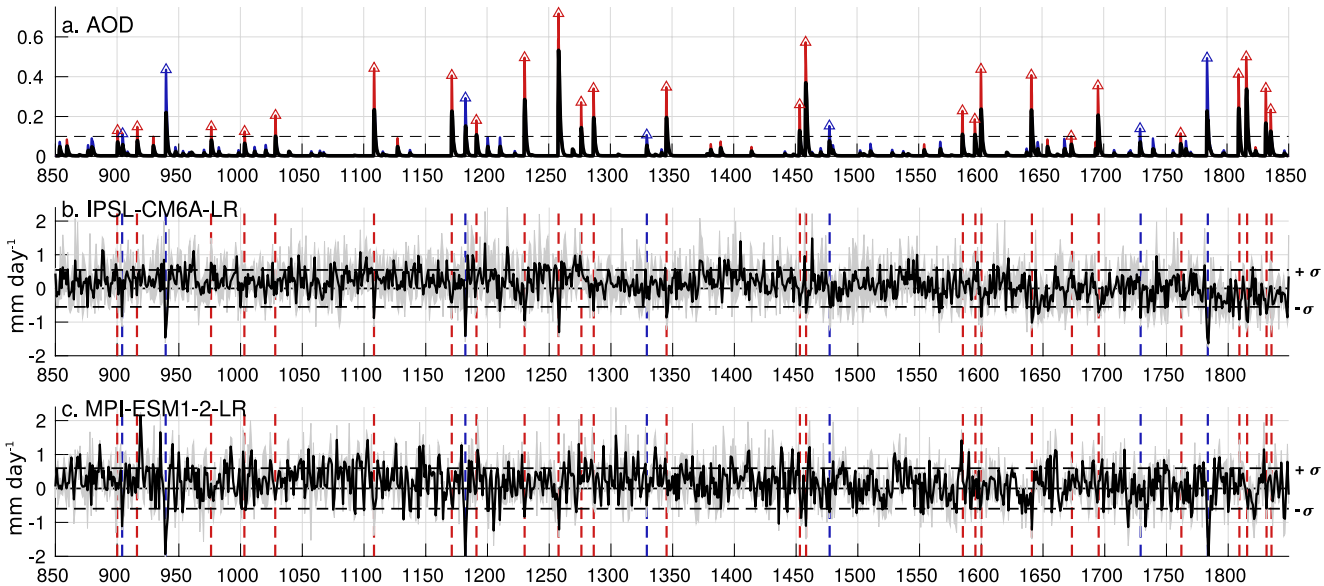

Figure 1. Volcanic forcing and Sahel rainfall anomalies between July and September in past1000 simulations. (a) Mean aerosol optical depth averaged (black) globally, (red) over the tropical (TROP) and (blue) extra-tropical NH (ETNH) ranges. Selection of (red triangles) TROP and (blue triangles) ETNH eruptions, exceeding (horizontal dashed line) the 0.1 threshold, extended as dashed vertical lines in (b, c). (b, c) Sahel precipitation index (SAHELPI) (mm day^{-1}) of (black indices) the three- and two-member ensemble-mean for respectively the IPSL-CM6A-LR and MPI-ESM1-2-LR models and (gray shading) ensemble spread. Horizontal dashed lines indicate the $\pm\sigma$ (standard deviation) of the piControl SAHELPI.

A moist static energy (MSE) decomposition (Pu & Cook, 2012) is performed to evaluate the convective local precipitation over central Sahel (10°W–10°E; 10°N–17.5°N) by decomposing it to the sensible heat (c_pT), the latent heat (Lq) and the potential energy (gz) components:

$$\mathrm{MSE} = c_pT + Lq + gz;$$

where T, q, and z are the temperature, the specific humidity and the geopotential height, respectively, averaged over the central Sahel area. c_p is the specific heat of dry air at constant pressure, L is the latent heat of vapourization of water at 0°C and g the gravitational acceleration.

3. Results

3.1. Sahel Inter-Annual Response to Volcanic Eruptions

The selection and classification of strong volcanic eruptions based on the AOD result in 7 ETNH and 26 TROP events (Figure 1, Table S2 in Supporting Information S1), with respectively strongly asymmetric and broadly symmetric hemispheric distributions of the radiative forcing (Figure S1 in Supporting Information S1). By matching the past1000 SAHELPI anomalies represented by all models with the selected eruptions events, it is noticeable that intense dry anomalies emerge following most of the large volcanic eruptions with different amplitudes that could be related to latitudes, season and magnitude of the events (Figures 1b and 1c). ETNH eruptions seem to induce larger Sahel rainfall response than TROP ones, even though the strongest eruptions in the CE are TROP events (e.g., the 1258 eruption; Figure 1a).

In order to analyze the different Sahel precipitation sensitivity simulated by the IPSL-CM6A-LR and MPI-ESM1-2-LR models to ETNH and TROP eruptions, the relationship between post-eruption JAS precipitation anomalies and the amplitude of the volcanic radiative forcing is represented in Figures 2a and 2b. Both models represent a similar linear relationship to ETNH eruptions with a significant precipitation response emerging from the internal variability when the global radiative imbalance exceeds about 1 W m^{-2}. However, the sensitivity to TROP eruptions differs across the two models. The radiative forcing has to be larger than 4 and 11 W m^{-2} for respectively IPSL-CM6A-LR and MPI-ESM1-2-LR to exert a significant drying which amplitude increases linearly with the eruption magnitude ($R^2 \sim 0.6$ for TROP and 0.7 for ETNH). Such uncertainty is

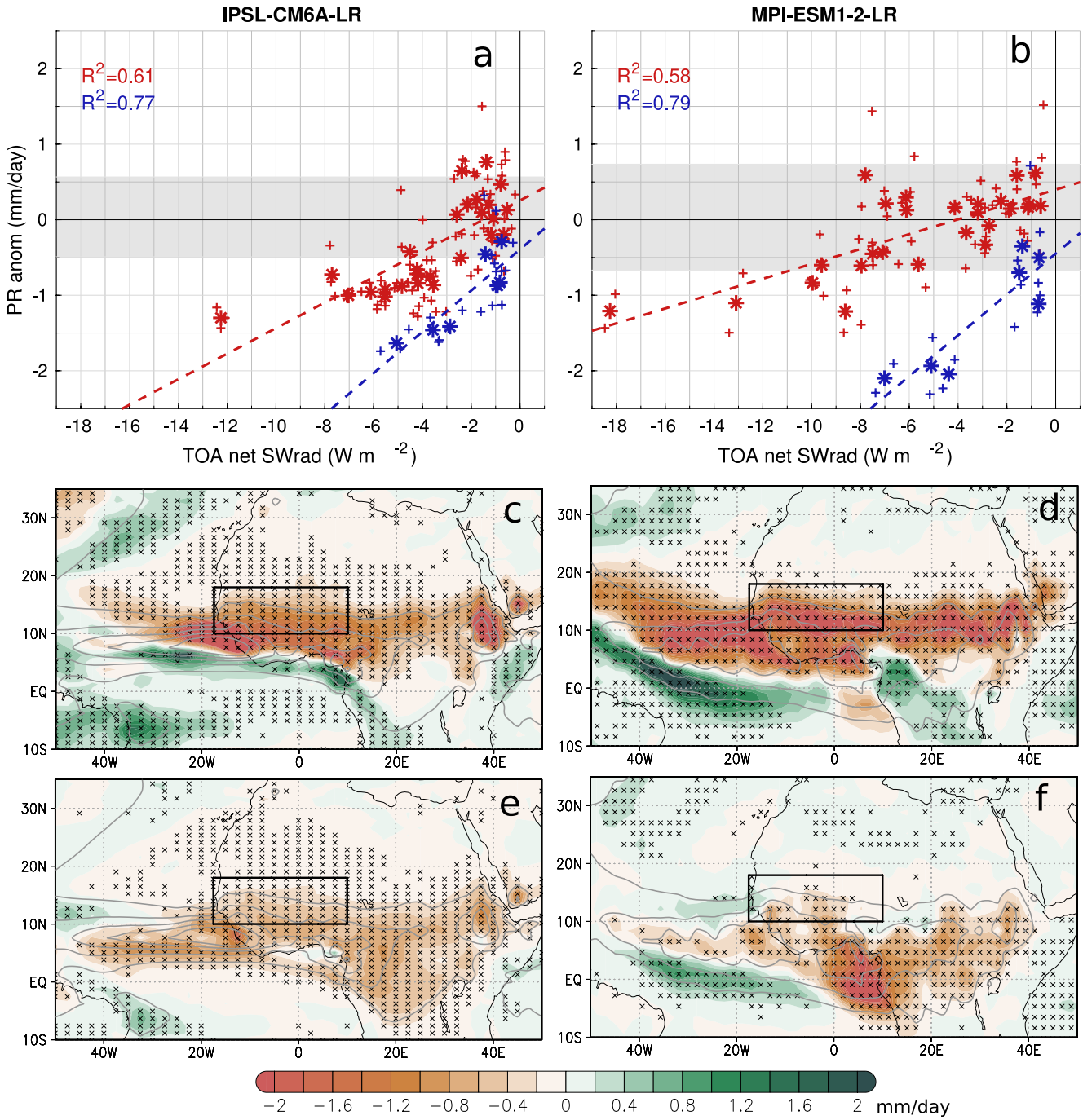

Figure 2. First post-eruption precipitation response between July and September to strong eruptions. (a, b) Linear relationship between Sahel precipitation and radiative forcing (asterisks) ensemble-mean and (crosses) individual-member anomalies corresponding to the selected (red) tropical (TROP) and (blue) extra-tropical NH (ETNH) volcanic events. (Gray shading) 95% confidence interval of the internal variability. (c, d) ETNH and (e, f) TROP composites of JAS precipitation anomalies the first post-eruption year (mm day^{-1}) and (contours) the climatology from 2 mm day^{-1} in intervals of 4 mm day^{-1}. Stippling indicates areas where the composite anomalies significantly emerge from the internal variability with 95% confidence level.

likely conditioned by the respective model biases in precipitation (Figure S3 in Supporting Information S1) and modulating factors. These results stress that the Sahel precipitation sensitivity is notably larger to ETNH than to TROP eruptions.

The ETNH-related composites maps of JAS precipitation show an anomalous tropical rain belt south of the climatological ITCZ position in both models (Figures 2c and 2d), while an overall drying over West Africa is

shown in TROP composites (Figures 2e and 2f). This suggests that the WAM reacts differently depending on the eruption latitude. We therefore investigate the different mechanisms at play during ETNH and TROP eruptions by analyzing the associated dynamics and thermodynamics in the following sections.

3.1.1. ETNH-Related Response

The time evolution of the Sahel rainfall response to ETNH eruptions is represented as composites of monthly anomalies over 3 years starting in the first post-eruption year (Figures 3a and 3b). They show significant negative anomalies during the two monsoon seasons following the eruptions (referred to as 1JAS and 2JAS seasons, respectively) robustly represented by both the IPSL-CM6A-LR and MPI-ESM1-2-LR models.

Associated with the 1JAS drying, a hemispheric contrast dominates the pattern of relative surface temperature composite anomalies (Figures 3c and 3d). Also, El Niño-like tropical Pacific warm anomalies and a strong land-sea contrast around West Africa are remarkable. These features are robustly represented by both the IPSL-CM6A-LR and MPI-ESM1-2-LR simulations and are consistent with Sahel drying (Grodsky et al., 2003; Nicholson, 2013). The atmospheric vertical profiles from both models show consistent anomalous southward shift of the local ITCZ over West Africa (i.e., mid-level convection around the equator along with strong subsidence roughly between 5°N and 20°N) along with the African Easterly Jet (Figures 3e and 3f). This mechanism, coherent with the anomalous meridional gradient of surface temperature, hinders the climatological northward intrusion of the tropical rain belt during the WAM season resulting in Sahel dry summers, in agreement with previous work (Dogar et al., 2017; Nicholson, 2013; Rowell et al., 1992). On the other hand, the El Niño-like relative SST pattern is associated with Walker circulation weakening and eastward shifting (Lau & Yang, 2003; Figure S4 in Supporting Information S1), coherent with 200-hPa velocity potential negative anomalies (i.e., high-level wind divergence) over the Pacific and positive anomalies (i.e., high-level wind convergence) over Africa (Figures 3c and 3d contour lines). This teleconnection induces widespread subsidence (Figure S4 in Supporting Information S1, left column) over the tropical Atlantic-western Indian ocean sector, which together with the southward ITCZ shift results in an overall West Africa drying and positive rainfall anomalies over Gulf of Guinea and equatorial Africa (Joly & Voldoire, 2009; Mohino, Rodríguez-Fonseca, et al., 2011). Similar but dimmed mechanisms are also found in 2JAS (Figure S5 in Supporting Information S1).

3.1.2. TROP-Related Response

In response to TROP eruptions, both the IPSL-CM6A-LR and the MPI-ESM1-2-LR past1000 simulations show negative precipitation anomalies in the 1JAS season (Figures 4a and 4b). However, the dry anomalies rarely exceed the threshold of internal variability significantly, given the aforementioned weaker sensitivity to TROP than to ETNH eruptions. The second post-eruption year significantly presents an anomalous early WAM onset robustly in both models in June (2Jun) and followed by a dry 2JAS season.

The TROP-related Sahel precipitation drying in 1JAS is associated with a pattern of relative surface temperatures with El Niño-like anomalies and pronounced land-sea contrast over West Africa. The tropical vertical profiles of both models show widespread subsidence and air-column drying all over West Africa, consistent with the El Niño-like Walker circulation anomalies (Janicot et al., 2001) and with tropical troposphere cooling in response to volcanic forcing, likely amplified by water vapor feedback (Soden et al., 2002) (Figure S4 in Supporting Information S1, right column; Figures 5c–5f). On the other hand, the land-sea temperature contrast between the Sahara and equatorial Atlantic is also associated with a WAM weakening (Grodsky et al., 2003; Nicholson, 2013) by dampening the inland pressure gradient that usually promotes the low-level monsoon flow in summer (Hourdin et al., 2010). In 2JAS, the responses are dimmed but consistent to 1JAS (Figure S6 in Supporting Information S1).

In 2Jun, positive Sahel precipitation anomalies are associated with a northward shift of the tropical rain belt (Figures 4g and 4h). The corresponding vertical profiles show an anomalous ITCZ shift compatible with an early onset of the Sahel rainy season (Figure S7 in Supporting Information S1), but cannot be explained by teleconnections with the relative SST pattern (not shown but similar to 1JAS and 2JAS). Therefore, we study the air-column thermodynamics over the Sahel relying on the MSE decomposition (Figures 4h–4j). MSE anomalies are associated with convective precipitation such that a negative MSE gradient with height denotes air column destabilization (Pu & Cook, 2012). Hence, the significant anomalies of the sensible heat (c_pT) component at around 500–300 hPa suggest the dominance of the intense upper-level troposphere cooling induced by TROP eruptions (Figure S4 in Supporting Information S1). This cooling is consistent with air-column instability favoring mid- and high-level deep convection (negative omega anomalies in Figures 4i and 4j; Nicholson, 2013) over the Sahel.

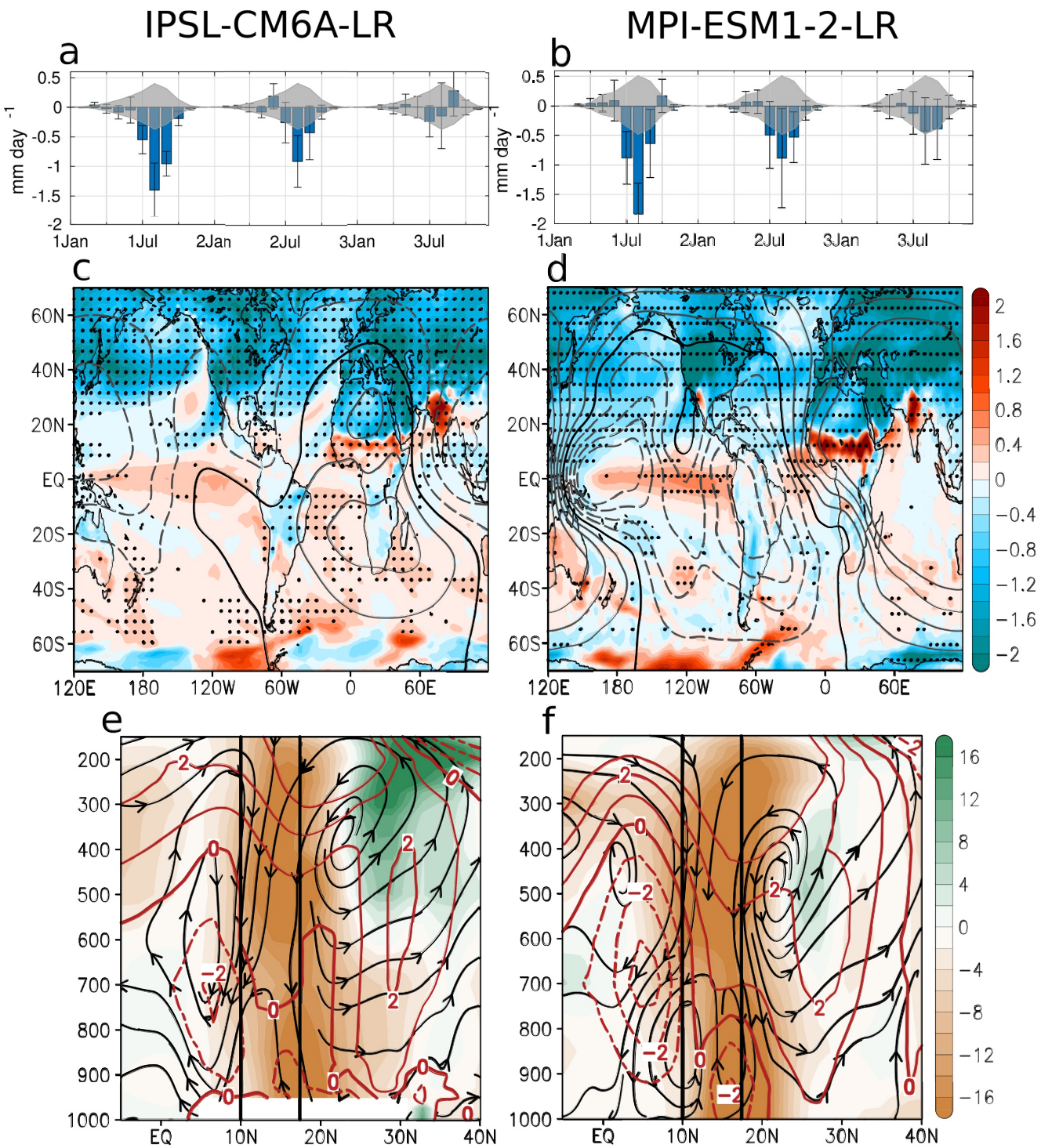

Figure 3. Extra-tropical NH-related composites of simulated (left column) IPSL-CM6A-LR and (right column) MPI-ESM1-2-LR post-eruption anomalies. (a, b) Timing of (bar chart) ensemble-mean monthly anomalies of Sahel precipitation, 95% confidence interval of (gray shade) the internal noise and (error bars) the spread across composite members. (c, d) Composites of 1JAS anomalies of (shade colors) relative surface temperature in °C and (contours) velocity potential at 200 hPa in intervals of 4×10^6 m^2 s^{-1}. (Stippling) Areas where the composite anomalies of relative temperature are statistically significant with a 95% confidence level. (e, f) Vertical profiles of 10°W–10°E averaged anomalies of (black streamlines) meridional-vertical wind, (red contours) zonal wind in m s^{-1} and (shade) relative anomalies of specific humidity in %.

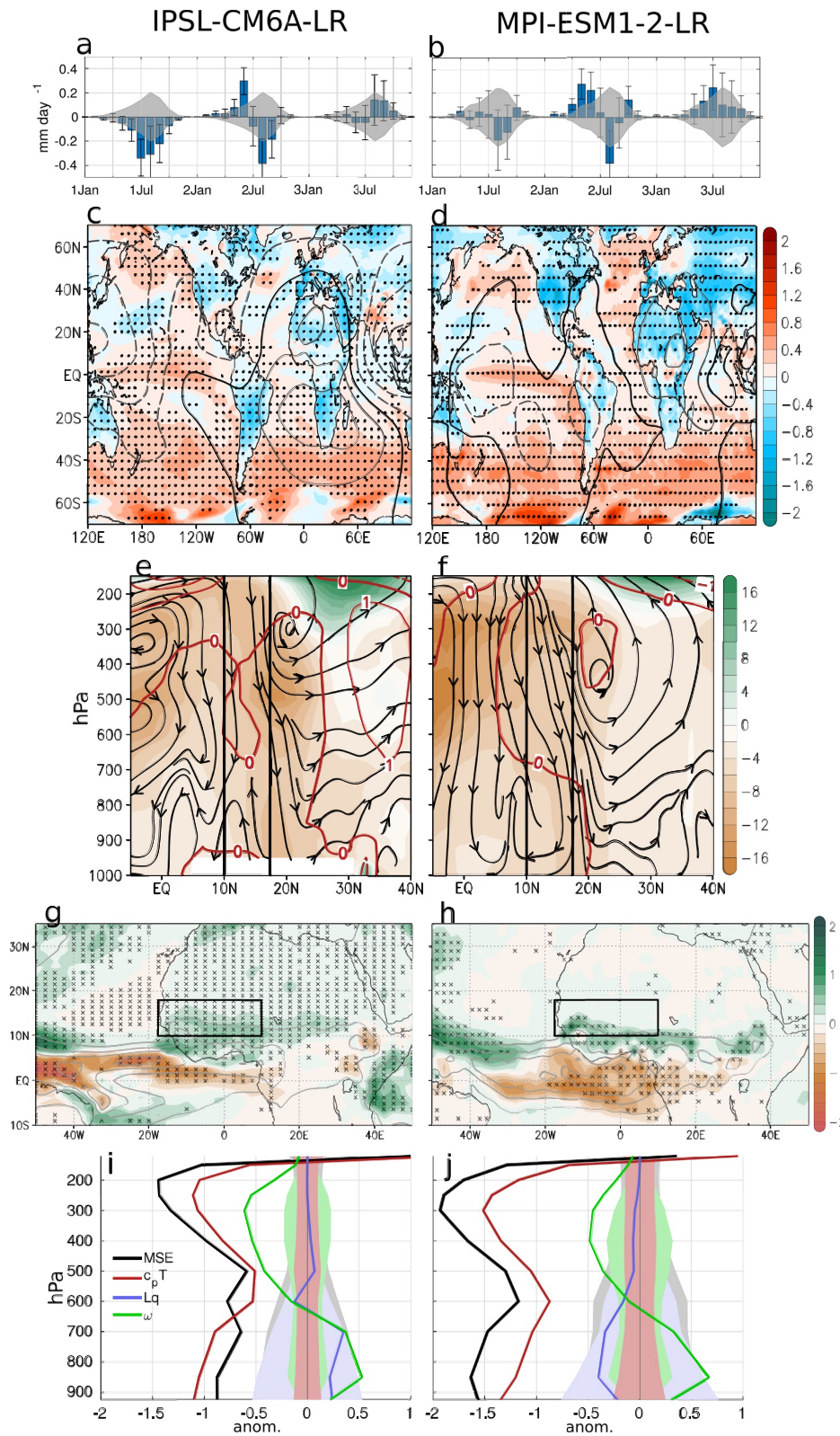

Figure 4. Tropical (TROP) composites of (left column) the IPSL-CM6A-LR and (right column) the MPI-ESM1-2-LR. (a–f) Same as Figure 3 but for TROP composites. (g, h) 2Jun composites of precipitation anomalies in mm day^{-1} (equivalent to Figures 2c–2f). (i, j) 2Jun anomalies of (black) the total moist static energy profile, (red) the sensible and (blue) latent heat components (units are kJ kg^{-1}), and (green) the omega vertical flow (units are hPa s^{-1}). Colored shadings indicate the 95% confidence intervals.

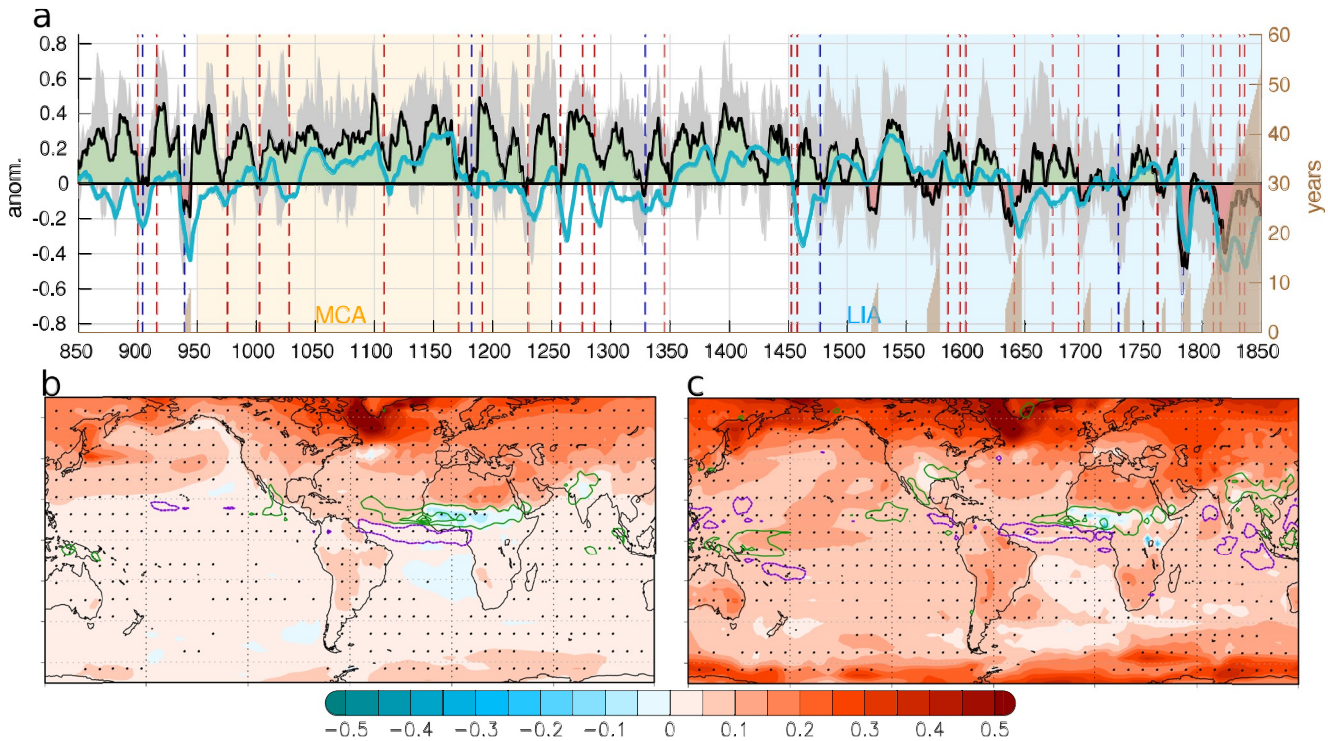

Figure 5. Decadal-to-secular variability of the model-mean Sahel precipitation. (a) (Green/red areas) Positive/negative anomalies of the (black line) 10-year low-pass-filtered Sahel precipitation index (SAHELPI) (mm day^{-1}) averaged across two members of the IPSL-CM6A-LR and MPI-ESM1-2-LR past1000 simulations (total spread in gray shade). (Blue index) model-mean forced Atlantic Multi-decadal Variability (AMV) index (i.e., "AMV-Residual" index from Fang et al. (2021)) in units of one standard deviation. (Brown shading) index of long-term drought persistence, that is, duration in years (right axis) of the filtered SAHELPI negative phases persisting above 5 years. Vertical dashed lines as in Figure 1. (b) Model-mean regression of standardized filtered SAHELPI on (colors) annual surface temperature anomalies in °C per std. dev. and (green/purple contours) positive/negative precipitation anomalies between July and September. (c) (Colors) Difference between the Medieval Climate Anomaly (950–1249) and the Little Ice Age (1450–1849) mean surface temperature in °C and (green/purple contours) positive/negative JAS precipitation anomalies. Stippling areas: full agreement of temperature anomalies sign across members. Precipitation contours: from ±0.1 in intervals of ±0.2 (b) mm day^{-1} per std. dev. or (c) mm day^{-1}.

These results suggest that the WAM responds to TROP events with reduced convection over West Africa through teleconnection with El Niño-like tropical Pacific SST the first post-eruption rainy season. The following year, the upper troposphere radiative cooling promotes an early Sahel rainy season, which turns out to be short due to a similar teleconnection as in 1JAS.

3.2. Sahel Multi-Decadal to Secular Response to Volcanic Eruptions

In this section, we explore the role of volcanic forcing over the past millennium Sahel precipitation multi-decadal variability. As both the ETNH and TROP eruptions are found to induce Sahel drought the following couple of years, we expect that high volcanic activity over long periods may modulate long-term changes on precipitation. In particular, the AMV, which affects the multi-decadal variability of the Sahel precipitation (e.g., Martin & Thorncroft, 2014; Mohino, Janicot, & Bader, 2011), can be impacted by volcanic eruptions in past1000 simulations (Fang et al., 2021).

The 10-year low pass filter SAHELPI from the IPSL-CM6A-LR and MPI-ESM1-2-LR multi-model mean (two members each for consistency) indicates a long-term component with 4% decline of the JAS precipitation in the Little Ice Age (LIA) with respect to the Medieval Climate Anomaly (MCA) (Figure 5a). The first centuries of the last millennium show relatively low volcanic activity until the 13th century and abundant Sahel precipitation. Then, after 1250, along with the increasing volcanic activity (Figure S8 in Supporting Information S1), a linear loss of JAS rainfall of −0.5 mm per decade is simulated until 1849. This suggests that increasing radiative imbalances triggered by strong volcanic eruptions over several centuries can induce a secular Sahel precipitation change toward a drier regime. The contrast between the MCA and the LIA (Figure 5c) is likely associated with an inter-hemispheric temperature contrast integrated by the ocean heat capacity favoring a gradual ITCZ southward

shift and a dipole of JAS precipitation anomalies spanning West Africa (Bischoff & Schneider, 2014; Schneider et al., 2014).

From the 16th century onwards, on top of the long-term trend, multi-decadal drought periods with larger amplitude emerge with a persistence that increases toward the late-18th and the mid-19th century (brown shading in Figure 5a; see also Figure S8a in Supporting Information S1). Such multi-decadal changes project on an AMV-like pattern of intense annual SST anomalies in the North Atlantic (Mohino, Janicot, & Bader, 2011) (Figure 5b). Our results are consistent with the recently reported contribution of volcanic forcing in the AMV signal in PMIP4/past1000 simulations (Fang et al., 2021). This forced AMV component (blue line in Figure 5a) significantly correlates with SAHELPI ($r = 0.28$, significant at the 1% level according to a random-phase test of Ebisuzaki (1997)), including those models with different volcanic forcing implementations (Figure S9 in Supporting Information S1) supporting a leading role of strong eruptions frequency (consistent across models) integrated by the ocean memory, rather than the short-term spatial distribution of the volcanic radiative forcing. The PMIP4/past1000 simulations further show a dramatic Sahel multi-decadal drought in the 19th century in agreement with historical reconstructions (Nicholson et al., 2012) that is unprecedented in amplitude and persistence since 850 AD. This result supports the hypothesis that the historical industrial period started from the Sahel driest decades of the past millennium, which was likely promoted by the closely spaced extra-tropical Laki event in 1783 CE and the tropical eruptions cluster over 1809–1835 CE before the anthropogenic effects came into play (Herman et al., 2020; Figure S9 in Supporting Information S1).

4. Summary

With past1000 simulations, this study shows WAM reactions to strong ETNH and TROP eruptions respectively associated with different mechanisms, up to two years after the event. A larger sensitivity of Sahel precipitation to ETNH than to TROP eruptions is found, both resulting in droughts whose magnitude is linearly related to the eruption strength.

ETNH-related drought in the two rainy seasons following a major eruption is controlled by the combined influence of El Niño-like teleconnection and an anomalous ITCZ southward shift due to surface temperature inter-hemispheric contrast in response to the asymmetric volcanic radiative forcing. TROP eruptions also lead to Sahel drought in the first following rainy season but an early and short rainy season in the second year. The TROP-induced WAM weakening is associated with ENSO teleconnections while the pre-onsetting of the second rainy season is due to the intense radiative cooling of the tropical troposphere.

We also identify and discuss multi-decadal-to-secular Sahel precipitation changes associated with volcanic forcing in past1000 simulations. These results suggest that the larger LIA multi-decadal variability is a consequence of the integration of the volcanic forcing in the AMV (Fang et al., 2021) through the modulation of the ITCZ meridional shifts over West Africa. Increasing volcanic activity over the late past millennium is also suggested to promote a secular drift of the Sahel precipitation regime toward drier conditions that culminated in the 19th century.

Data Availability Statement

Models used in this work are listed in Table S1 in Supporting Information S1. Data supporting the findings of this study are available at: https://esgf-node.ipsl.upmc.fr/search/cmip6-ipsl/.

Acknowledgments
We thank the editor Dr. Giannini and the three anonymous reviewers for their constructive comments that helped improve this manuscript. This work was undertaken in the framework of the French L-IPSL LABEX and the IPSL Climate Graduate School EUR and benefited from the FNS "SYNERGIA EffeCts of lArge voLcanic eruptions on climate and societies: UnDerstanding impacts of past Events and related subsidence cRises to evaluate potential risks in the future" (CALDERA) project under French CNRS grant agreement number CRSII5_183571—CALDERA. The authors acknowledge the World Climate Research Programme's Working Group on Coupled Modelling, which is responsible for PMIP and CMIP. MK acknowledges support from the HPC resources of TGCC under the allocations 2020-A0080107732 and 2021-A0100107732 (project GENCMIP6) provided by GENCI (Grand Equipment National de Calcul Intensif) and 2020225424 provided by PRACE (Partnership for Advanced Computing in Europe). This study benefited from the ESPRI computing and data center (https://mesocentre.ipsl.fr) which is supported by CNRS, Sorbonne Université, Ecole Polytechnique and CNES as well as through national and international grants. S-W.F. is funded by the German Federal Ministry of Education and Research (BMBF), research programme "ROMIC-II, ISOVIC" (FKZ: 01LG1909B). C.T. is funded by the Deutsche Forschung Gemeinschaft (DFG) research unit FOR 2820: VolImpact, (Grant: 398006378). The MPI-ESM computations, analysis and model data storage were performed at the Deutsches Klima Rechenzentrum (DKRZ).

References

Ackerley, D., Booth, B. B. B., Knight, S. H. E., Highwood, E. J., Frame, D. J., Allen, M. R., & Rowell, D. P. (2011). Sensitivity of twentieth-century Sahel rainfall to sulfate aerosol and CO_2 forcing. *Journal of Climate*, *24*(19), 4999–5014. https://doi.org/10.1175/JCLI-D-11-00019.1

Biasutti, M. (2013). Forced Sahel rainfall trends in the CMIP5 archive. *Journal of Geophysical Research: Atmospheres*, *118*(4), 1613–1623. https://doi.org/10.1002/jgrd.50206

Bischoff, T., & Schneider, T. (2014). Energetic constraints on the position of the intertropical convergence zone. *Journal of Climate*, *27*(13), 4937–4951. https://doi.org/10.1175/JCLI-D-13-00650.1

Boucher, O., Servonnat, J., Albright, A. L., Aumont, O., Balkanski, Y., Bastrikov, V., et al. (2020). Presentation and evaluation of the IPSL-CM6A-LR climate model. *Journal of Advances in Modeling Earth Systems*, *12*(7), 1–52. https://doi.org/10.1029/2019MS002010

Colose, C. M., LeGrande, A. N., & Vuille, M. (2016). Hemispherically asymmetric volcanic forcing of tropical hydroclimate during the last millennium. *Earth System Dynamics*, *7*(3), 681–696. https://doi.org/10.5194/esd-7-681-2016

D'Agostino, R., & Timmreck, C. (2022). Sensitivity of regional monsoons to idealised equatorial volcanic eruption of different sulfur emission strengths. *Environmental Research Letters*, *17*(5), 054001. https://doi.org/10.1088/1748-9326/ac62af

Dogar, M. M., Stenchikov, G., Osipov, S., Wyman, B., & Zhao, M. (2017). Sensitivity of the regional climate in the Middle East and North Africa to volcanic perturbations. *Journal of Geophysical Research: Atmospheres*, *122*(15), 7922–7948. https://doi.org/10.1002/2017jd026783

Ebisuzaki, W. (1997). A method to estimate the statistical significance of a correlation when the data are serially correlated. *Journal of Climate*, *10*(9), 2147–2153. https://doi.org/10.1175/1520-0442(1997)010<2147:amtets>2.0.co;2

Erez, M., & Adam, O. (2021). Energetic constraints on the time-dependent response of the ITCZ to volcanic eruptions. *Journal of Climate*, *34*(24), 9989–10006. https://doi.org/10.1175/JCLI-D-21-0146.1

Eyring, V., Bony, S., Meehl, G. A., Senior, C. A., Stevens, B., Stouffer, R. J., & Taylor, K. E. (2016). Overview of the Coupled Model Intercomparison Project Phase 6 (CMIP6) experimental design and organization. *Geoscientific Model Development*, *9*(5), 1937–1958. https://doi.org/10.5194/gmd-9-1937-2016

Fang, S. W., Khodri, M., Timmreck, C., Zanchettin, D., & Jungclaus, J. (2021). Disentangling internal and external contributions to Atlantic multidecadal variability over the past millennium. *Geophysical Research Letters*, *48*(23), 1–10. https://doi.org/10.1029/2021GL095990

Folland, C. K., Palmer, T. N., & Parker, D. E. (1986). Sahel rainfall and worldwide sea temperatures, 1901–85. *Nature*, *320*(6063), 602–607. https://doi.org/10.1038/320602a0

Gaetani, M., Flamant, C., Bastin, S., Janicot, S., Lavaysse, C., Hourdin, F., et al. (2017). West African monsoon dynamics and precipitation: The competition between global SST warming and CO_2 increase in CMIP5 idealized simulations. *Climate Dynamics*, *48*(3–4), 1353–1373. https://doi.org/10.1007/s00382-016-3146-z

Gallego, D., Ordóñez, P., Ribera, P., Peña-Ortiz, C., & García-Herrera, R. (2015). An instrumental index of the West African Monsoon back to the nineteenth century. *Quarterly Journal of the Royal Meteorological Society*, *141*(693), 3166–3176. https://doi.org/10.1002/qj.2601

Giannini, A., Saravanan, R., & Chang, P. (2003). Oceanic forcing of Sahel rainfall on interannual to interdecadal time scales. *Science*, *302*(5647), 1027–1030. https://doi.org/10.1126/science.1089357

Grodsky, S. A., Carton, J. A., & Nigam, S. (2003). Near surface westerly wind jet in the Atlantic ITCZ. *Geophysical Research Letters*, *30*(19), 3–6. https://doi.org/10.1029/2003GL017867

Haywood, J. M., Jones, A., Bellouin, N., & Stephenson, D. (2013). Asymmetric forcing from stratospheric aerosols impacts Sahelian rainfall. *Nature Climate Change*, *3*(7), 660–665. https://doi.org/10.1038/nclimate1857

Herman, R. J., Giannini, A., Biasutti, M., & Kushnir, Y. (2020). The effects of anthropogenic and volcanic aerosols and greenhouse gases on twentieth century Sahel precipitation. *Scientific Reports*, *10*(1), 1–11. https://doi.org/10.1038/s41598-020-68356-w

Hourdin, F., Musat, I., Guichard, F., Ruti, P. M., Favot, F., Filiberti, M. A., et al. (2010). Amma-model intercomparison project. *Bulletin of the American Meteorological Society*, *91*(1), 95–104. https://doi.org/10.1175/2009BAMS2791.1

Jacobson, T. W. P., Yang, W., Vecchi, G. A., & Horowitz, L. W. (2020). Impact of volcanic aerosol hemispheric symmetry on Sahel rainfall. *Climate Dynamics*, *55*(7–8), 1733–1758. https://doi.org/10.1007/s00382-020-05347-7

Janicot, S., Trzaska, S., & Poccard, I. (2001). Summer Sahel-ENSO teleconnection and decadal time scale SST variations. *Climate Dynamics*, *18*(3–4), 303–320. https://doi.org/10.1007/s003820100172

Joly, M., & Voldoire, A. (2009). Influence of ENSO on the West African monsoon: Temporal aspects and atmospheric processes. *Journal of Climate*, *22*(12), 3193–3210. https://doi.org/10.1175/2008JCLI2450.1

Jungclaus, J. H., Bard, E., Baroni, M., Braconnot, P., Cao, J., Chini, L. P., et al. (2017). The PMIP4 contribution to CMIP6—Part 3: The last millennium, scientific objective, and experimental design for the PMIP4 past1000 simulations. *Geoscientific Model Development*, *10*(11), 4005–4033. https://doi.org/10.5194/gmd-10-4005-2017

Kageyama, M., Braconnot, P., Harrison, S. P., Haywood, A. M., Jungclaus, J. H., Otto-Bliesner, B. L., et al. (2018). The PMIP4 contribution to CMIP6—Part 1: Overview and over-arching analysis plan. *Geoscientific Model Development*, *11*(3), 1033–1057. https://doi.org/10.5194/gmd-11-1033-2018

Khodri, M., Izumo, T., Vialard, J., Janicot, S., Cassou, C., Lengaigne, M., et al. (2017). Tropical explosive volcanic eruptions can trigger El Ninõ by cooling tropical Africa. *Nature Communications*, *8*(1), 1–12. https://doi.org/10.1038/s41467-017-00755-6

Knight, J. R., Folland, C. K., & Scaife, A. A. (2006). Climate impacts of the Atlantic multidecadal oscillation. *Geophysical Research Letters*, *33*(17), L17706. https://doi.org/10.1029/2006GL026242

Kucharski, F., Molteni, F., King, M. P., Farneti, R., Kang, I.-S., & Feudale, L. (2013). On the need of intermediate complexity general circulation models: A "SPEEDY" example. *Bulletin of the American Meteorological Society*, *94*(1), 25–30. https://doi.org/10.1175/BAMS-D-11-00238.1

Lau, K.-M., & Yang, S. (2003). Walker circulation. In *Encyclopedia of atmospheric sciences* (pp. 2505–2510). https://doi.org/10.1006/rwas.2002.0450

Lüning, S., Gałka, M., Danladi, I. B., Adagunodo, T. A., & Vahrenholt, F. (2018). Hydroclimate in Africa during the medieval climate anomaly. *Palaeogeography, Palaeoclimatology, Palaeoecology*, *495*, 309–322. https://doi.org/10.1016/j.palaeo.2018.01.025

Lurton, T., Balkanski, Y., Bastrikov, V., Bekki, S., Bopp, L., Braconnot, P., et al. (2020). Implementation of the CMIP6 forcing data in the IPSL-CM6A-LR model. *Journal of Advances in Modeling Earth Systems*, *12*(4), 1–22. https://doi.org/10.1029/2019MS001940

Man, W., Zuo, M., Zhou, T., Fasullo, J. T., Bethke, I., Chen, X., et al. (2021). Potential influences of volcanic eruptions on future global land monsoon precipitation changes. *Earth's Future*, *9*(3), 1–14. https://doi.org/10.1029/2020EF001803

Manning, J. G., Ludlow, F., Stine, A. R., Boos, W. R., Sigl, M., & Marlon, J. R. (2017). Volcanic suppression of Nile summer flooding triggers revolt and constrains interstate conflict in ancient Egypt. *Nature Communications*, *8*(1), 1–8. https://doi.org/10.1038/s41467-017-00957-y

Martin, E. R., & Thorncroft, C. D. (2014). The impact of the AMO on the West African monsoon annual cycle. *Quarterly Journal of the Royal Meteorological Society*, *140*(678), 31–46. https://doi.org/10.1002/qj.2107

Mauritsen, T., Bader, J., Becker, T., Behrens, J., Bittner, M., Brokopf, R., et al. (2019). Developments in the MPI-M Earth system model version 1.2 (MPI-ESM1.2) and its response to increasing CO_2. *Journal of Advances in Modeling Earth Systems*, *11*(4), 998–1038. https://doi.org/10.1029/2018MS001400

McGregor, H. V., Evans, M. N., Goosse, H., Leduc, G., Martrat, B., Addison, J. A., et al. (2015). Robust global ocean cooling trend for the pre-industrial Common Era. *Nature Geoscience*, *8*(9), 671–677. https://doi.org/10.1038/ngeo2510

Mohino, E., Janicot, S., & Bader, J. (2011). Sahel rainfall and decadal to multi-decadal sea surface temperature variability. *Climate Dynamics*, *37*(3–4), 419–440. https://doi.org/10.1007/s00382-010-0867-2

Mohino, E., Rodríguez-Fonseca, B., Mechoso, C. R., Gervois, S., Ruti, P., & Chauvin, F. (2011). Impacts of the tropical Pacific/Indian oceans on the seasonal cycle of the west african monsoon. *Journal of Climate*, *24*(15), 3878–3891. https://doi.org/10.1175/2011JCLI3988.1

Nicholson, S. E. (2013). The West African Sahel: A review of recent studies on the rainfall regime and its interannual variability. *ISRN Meteorology*, *2013*(453521), 32. https://doi.org/10.1155/2013/453521

Nicholson, S. E., Klotter, D., & Dezfuli, A. K. (2012). Spatial reconstruction of semi-quantitative precipitation fields over Africa during the nineteenth century from documentary evidence and gauge data. *Quaternary Research*, *78*(1), 13–23. https://doi.org/10.1016/j.yqres.2012.03.012

Oman, L., Robock, A., Stenchikov, G. L., & Thordarson, T. (2006). High-latitude eruptions cast shadow over the African monsoon and the flow of the Nile. *Geophysical Research Letters*, *33*(18), 1–5. https://doi.org/10.1029/2006GL027665

Park, J.-Y., Bader, J., & Matei, D. (2015). Northern-hemispheric differential warming is the key to understanding the discrepancies in the projected Sahel rainfall. *Nature Communications*, *6*(1), 5985. https://doi.org/10.1038/ncomms6985

Pu, B., & Cook, K. H. (2012). Role of the West African westerly jet in Sahel rainfall variations. *Journal of Climate*, *25*(8), 2880–2896. https://doi.org/10.1175/JCLI-D-11-00394.1

Robock, A. (2000). Volcanic eruptions and climate. *Reviews of Geophysics*, *38*(2), 191–219. https://doi.org/10.1029/1998rg000054

Rodríguez-Fonseca, B., Mohino, E., Mechoso, C. R., Caminade, C., Biasutti, M., Gaetani, M., et al. (2015). Variability and predictability of West African droughts: A review on the role of sea surface temperature anomalies. *Journal of Climate*, *28*(10), 4034–4060. https://doi.org/10.1175/JCLI-D-14-00130.1

Rowell, D. P., Folland, C. K., Maskell, K., Owen, J. A., & Ward, M. N. (1992). Modelling the influence of global sea surface temperatures on the variability and predictability of seasonal Sahel rainfall. *Geophysical Research Letters*, *19*(9), 905–908. https://doi.org/10.1029/92gl00939

Schneider, T., Bischoff, T., & Haug, G. H. (2014). Migrations and dynamics of the intertropical convergence zone. *Nature*, *513*(7516), 45–53. https://doi.org/10.1038/nature13636

Soden, B. J., Wetherald, R. T., Stenchikov, G. L., & Robock, A. (2002). Global cooling after the eruption of mount Pinatubo: A test of climate feedback by water vapor. *Science*, *296*(5568), 727–730. https://doi.org/10.1126/science.296.5568.727

Tejedor, E., Steiger, N. J., Smerdon, J. E., Serrano-Notivoli, R., & Vuille, M. (2021). Global hydroclimatic response to tropical volcanic eruptions over the last millennium. *Proceedings of the National Academy of Sciences of the United States of America*, *118*(12), 1–9. https://doi.org/10.1073/pnas.2019145118

Timmreck, C. (2012). Modeling the climatic effects of large explosive volcanic eruptions. *Wiley Interdisciplinary Reviews: Climate Change*, *3*(6), 545–564. https://doi.org/10.1002/wcc.192

Toohey, M., & Sigl, M. (2017). Volcanic stratospheric sulfur injections and aerosol optical depth from 500 BCE to 1900 CE. *Earth System Science Data*, *9*(2), 809–831. https://doi.org/10.5194/essd-9-809-2017

Toohey, M., Stevens, B., Schmidt, H., & Timmreck, C. (2016). Easy volcanic aerosol (EVA v1.0): An idealized forcing generator for climate simulations. *Geoscientific Model Development*, *9*(11), 4049–4070. https://doi.org/10.5194/gmd-9-4049-2016

van Dijk, E., Jungclaus, J., Lorenz, S., Timmreck, C., & Krüger, K. (2022). Was there a volcanic-induced long-lasting cooling over the Northern Hemisphere in the mid-6th–7th century? *Climate of the Past*, *18*(7), 1601–1623. https://doi.org/10.5194/cp-18-1601-2022

Zeng, N., & Neelin, J. D. (1999). A land-atmosphere interaction theory for the tropical deforestation problem. *Journal of Climate*, *12*, 857–872.

References From the Supporting Information

Hajima, T., Abe, M., Arakawa, O., Suzuki, T., Komuro, Y., & Ogura, T. (2019). *MIROC MIROC-ES2L model output prepared for CMIP6 CMIP piControl. Version 20191230* (p. 5710). Earth System Grid Federation.

Ohgaito, R., Yamamoto, A., Hajima, T., O'Ishi, R., Abe, M., Tatebe, H., et al. (2021). PMIP4 experiments using MIROC-ES2L Earth system model. *Geoscientific Model Development*, *14*(2), 1195–1217. https://doi.org/10.5194/gmd-14-1195-2021

Schneider, U., Becker, A., Finger, P., Rustemeier, E., & Ziese, M. (2020). GPCC full data monthly product version 2020 at 0.25°: Monthly land-surface precipitation from rain-Gauges built on GTS-based and historical data. In *Global Precipitation Climatology Centre (GPCC) at Deutscher Wetterdienst*.

Yukimoto, S., Kawai, H., Koshiro, T., Oshima, N., Yoshida, K., Urakawa, S., et al. (2019). The meteorological research institute Earth system model version 2.0, MRI-ESM2.0: Description and basic evaluation of the physical component. *Journal of the Meteorological Society of Japan*, *97*(5), 931–965. https://doi.org/10.2151/jmsj.2019-051